Copper doped magnetic vortex nanoring based nanotherapeutics for bacterial infection tri-therapy: interplay of magnetic hyperthermia, chemodynamic and photothermal therapy

Jing Wang,[†a] Wenqian Zhao, [†a] Hui Tu,[a] Xiangyang Zu,[a] Jinghua Li,[a] Kun Lei,[a] Jing Li,[b] Yuchuan Zhuang, [c] Yanbo Dong, [d] Andrey Tulupov, [e] Fengshou Zhang *[a] and Jianfeng Bao *[a]

a. School of Medical Technology and Engineering, Henan University of Science and Technology, Luoyang 71000, China.

b. Office of Science and Technology, Henan University of Science and Technology, Luoyang, China.3. Office of Science and Technology, Henan University of Science and Technology, Luoyang, China.

c. Department of Imaging Sciences, University of Rochester Medical Center, Rochester, NY, United States.

d. Faculty of Teacher Education, Pingdingshan University, Pingdingshan, Henan, 467000, People's Republic of China.

e. Laboratory of MRT technologies, The Institute International Tomography Center of the Russian Academy of Sciences, Institutskaya Str. 3A, 630090, Novosibirsk, Russia.

SUPPORTING INFORMATION

Table of Content

S1: SEM images of MVN ,MVNp and Cu-MVNp

Evaluate the morphology of synthesized MVN, MVNp and Cu-MVNp by using SEM.
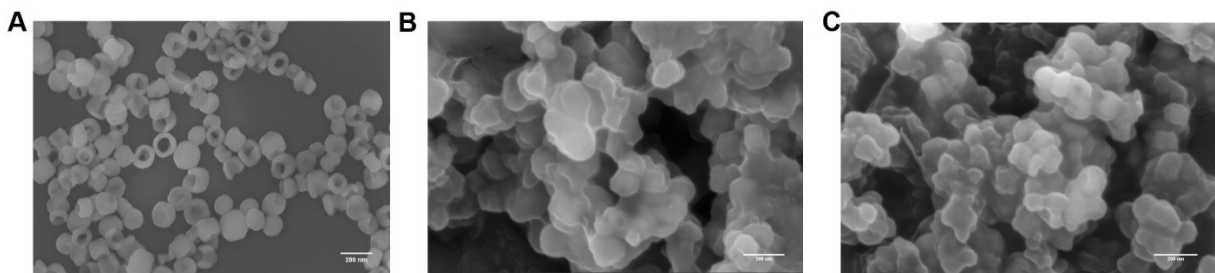
Fig. S1 The SEM images of (A) MVN (B) MVNp and (C) Cu-MVNp (Scale bars: 200 nm).

S2: Magnetic-thermal performance of the Cu-MVNp
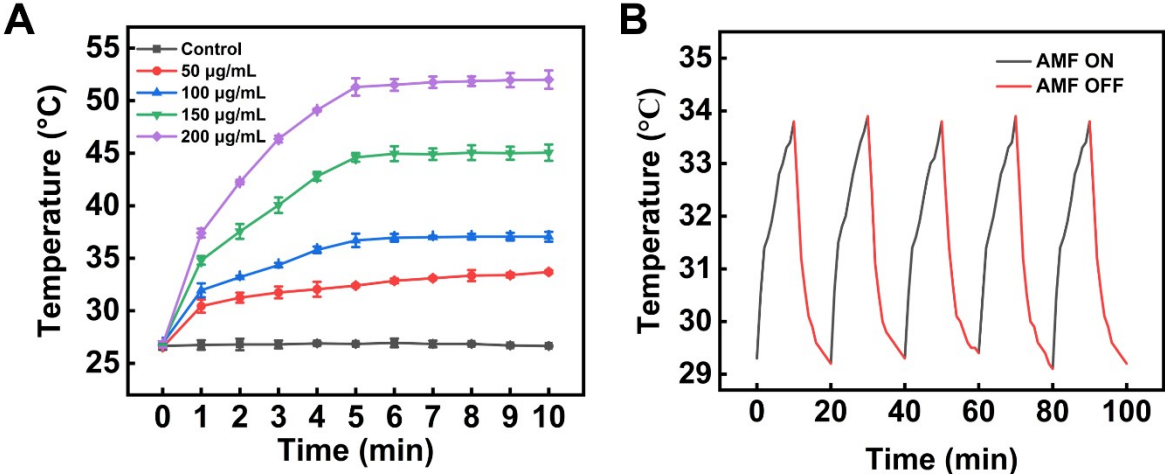
Fig. S2 (A) Heat-up curves of Cu-MVNp with different concentrations under AMF; (B) Magnetothermal stability of Cu-MVNp under AMF with 5 repeated cycles on/off.

S3: Photothermal properties studies

After diluting the Cu-MVNp solution, place it in sample bottles exposed to an 808 nm laser (1.5 W·cm⁻²) to obtain the photothermal images of the Cu-MVNp solution. Use a handheld thermal imaging camera to measure the solution temperature every 30 seconds.

According to Ren's report[1], the photothermal conversion efficiency (η) can be described by the following equation:

$$\eta = \frac{hA\left(\Delta T_{max} - \Delta T_{max,H_2O}\right)}{I\left(1 - 10^{-A_\lambda}\right)} \tag{1}$$

In the context of containers, h represents the heat transfer coefficient, A denotes the surface area, and ΔT_{max} refers to the maximum temperature change in the Cu-MVNp solution under NIR irradiation. ΔT_{maxH_2O} indicates the temperature change of water under similar conditions. I stands for the near-infrared laser power density, and A_λ represents the light absorption coefficient of Cu-MVNp at 808 nm.

$$\tau_s = \frac{\Sigma_i m_i c_{p,i}}{hA} \tag{2}$$

Given that the mass of Cu-MVNp in the solution is significantly smaller than that of water, we can simplify the equation as follows:

$$\tau_s = \frac{m_{H_2O} c_{H_2O}}{hA} \tag{3}$$

Here, m_d represents the mass of water, c_{H_2O} is the specific heat capacity of water, and τ_s is the time constant, which can be determined using the following formula:

$$\tau_s = \frac{t}{-\ln\theta} \tag{4}$$

$$\theta = \frac{T_{surr} - T}{T_{surr} - T_{max}} \tag{5}$$

In these equations, t refers to the real-time cooling duration and T represents the real-time temperature at time t. Tsurr stands for the ambient temperature, and Tmax is the maximum stable temperature of the solution.

In these equations, t denotes the actual cooling duration, and T represents the real-time temperature at time t. T_{surr} refers to the ambient temperature, while T_{max} is the maximum stable temperature of the solution.

S4: Cu-MVNp is heated under the combined action of AMF and NIR
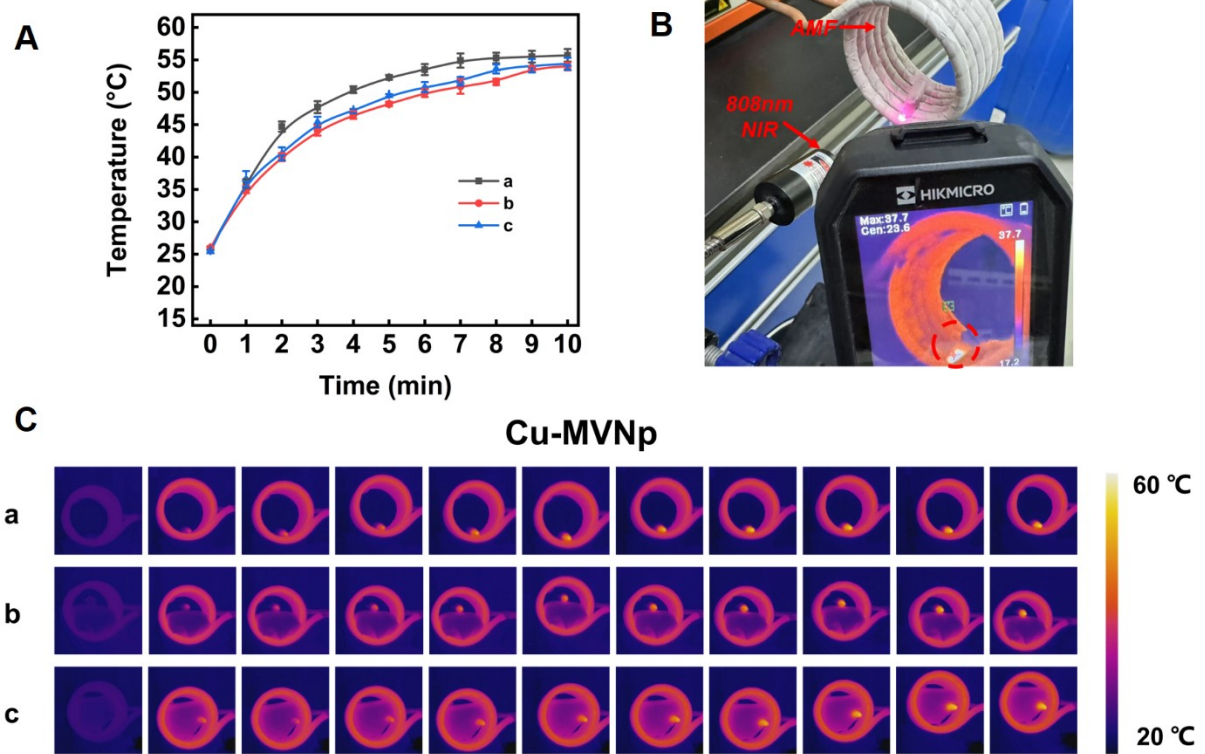
Fig. S3 (A) Temperature variations of Cu-MVNp (150 µg/mL) under the combined action of AMF (U = 220 V, f = 300 kHz, I = 30 A) and NIR (1.5 W/cm^2) (a: sample placed at the coil's edge; b: sample located at the center of the coil; c: sample positioned near the coil); (B) Digital photograph of the thermal imaging of Cu-MVNp solution under NIR irradiation and AMF exposure; (C) Infrared thermographic images of Cu-MVNp heating under the combined effects of AMF and NIR.

S5: In vitro photothermal antibacterial

Initially, we compared the inactivation effects of Cu-MVNp at various concentrations under NIR treatment on E. coli and S. aureus, with each group supplemented with 1 mM of H_2O_2. As depicted in Fig. S4A and B, when we set the 808 nm laser power to 1.5 W·cm^{-2} for 10 minutes, the mixed solution of Cu-MVNp at concentrations of 50, 75, 100, 150, and 200 µg/mL achieved temperatures of 44.8, 48.3, 59.0, 61.5, and 72.7°C, respectively, with E. coli. Conversely, the mixed solution with S. aureus reached temperatures of 44.6, 51.1, 59.7, 66.4, and 74.6°C. The plate count results in Fig. S4C and D indicated that solely adding Cu-MVNp had minimal inactivation effects on both E. coli and S. aureus. At a concentration of 150 µg/mL, NIR treatment exhibited significant ablation effects on both bacteria.

To identify the optimal laser treatment power, we examined the heating profile and antibacterial efficacy of Cu-MVNp at 150 µg/mL under different powers. As illustrated in Fig. S4E and F, at this concentration, the temperatures of the mixed solution with E. coli increased to 44.8, 47.8, 54.6, 55.8, and 66.8°C at laser powers of 0.6, 0.7, 0.8, 0.9, and 1.2 W·cm^{-2}, respectively. For the mixed solution with S. aureus, the temperatures rose to 39.3, 47.2, 53.4, 56.8, and 67.4°C. Plate count data demonstrated that Cu-MVNp at 150 µg/mL exhibited excellent antibacterial efficacy at a laser power of 0.8 W·cm^{-2}, achieving kill rates of 100% for both E. coli and S. aureus (Fig. S4G and H).
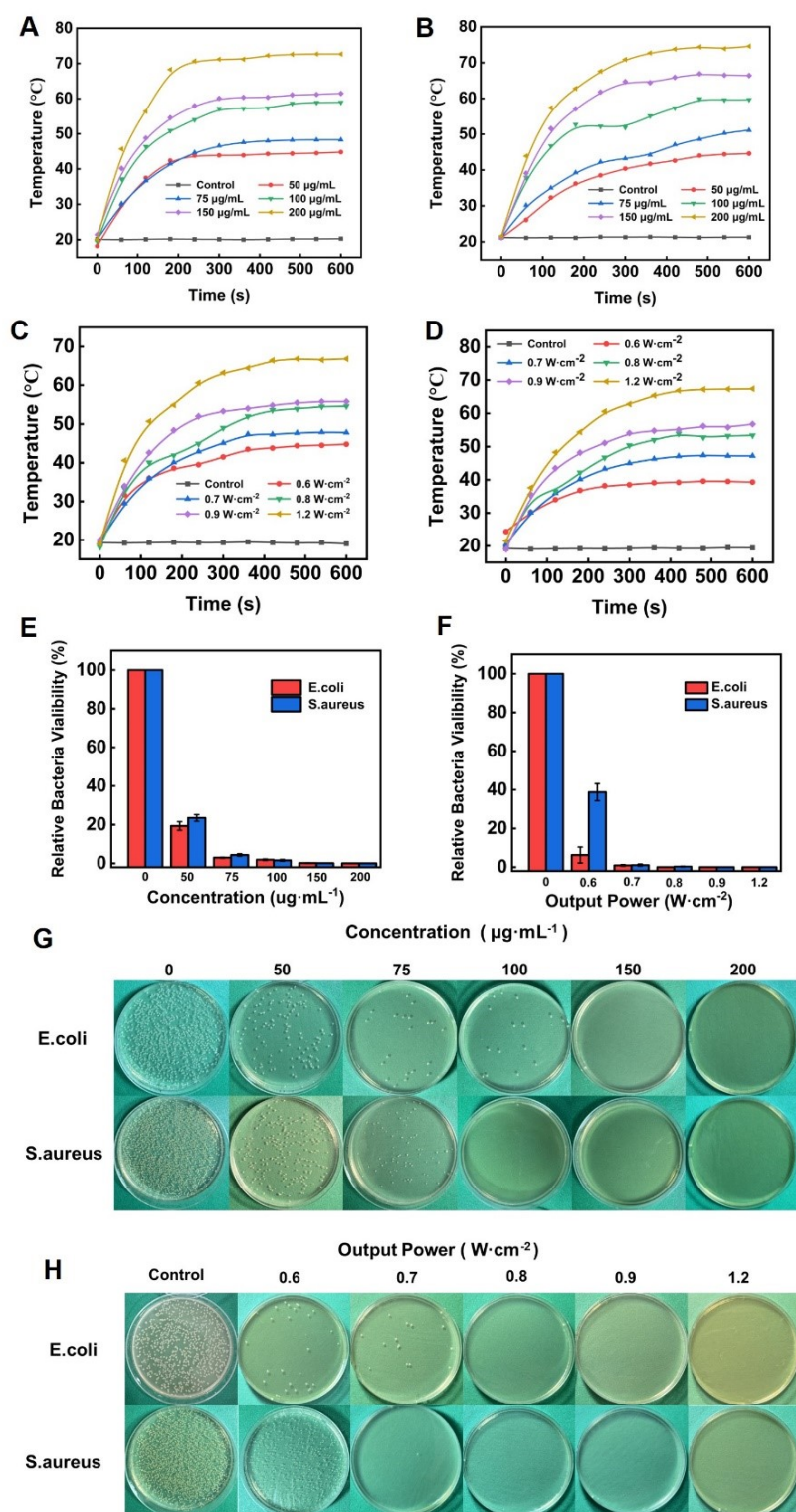
Fig. S4 (A) Temperature variations of E. coli (B) S. aureus under varying concentrations of Cu-MVNp exposed to near-infrared radiation (1.5 W·cm⁻²); (C) Temperature changes of E. coli (D) S. aureus mixed with 150 μg/mL Cu-MVNp at different near-infrared power levels; (E) Bacterial survival rates of E. coli and S. aureus post-treatment with different concentrations of Cu-MVNp; (F) Bacterial survival rates of E. coli and S. aureus after treatment with varying NIR power levels; (G) Antimicrobial effectiveness of different concentrations of Cu-MVNp on agar plates under near-infrared radiation (1.5 W·cm⁻²); (H) Colony images of E. coli and S. aureus at various laser power outputs.

S6: In vitro biocompatibility evaluation
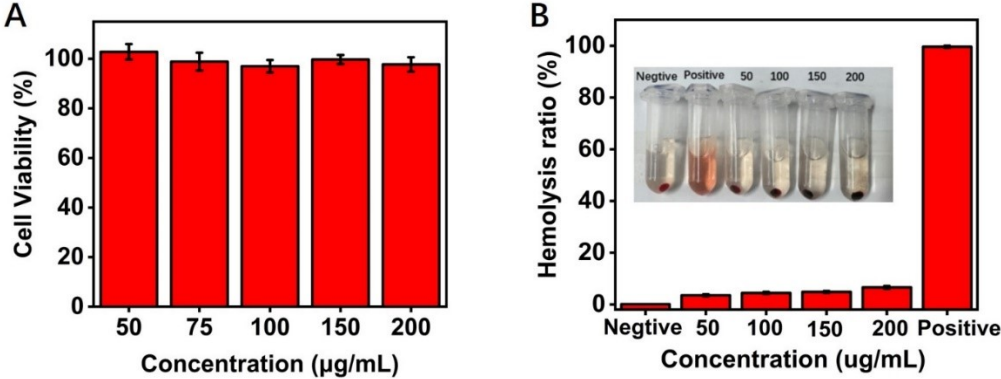
Fig. S5 (A) Cell safety experiments and (B) blood compatibility results of varying concentrations of Cu-MVNp.

S7: In vivo biosafety evaluation
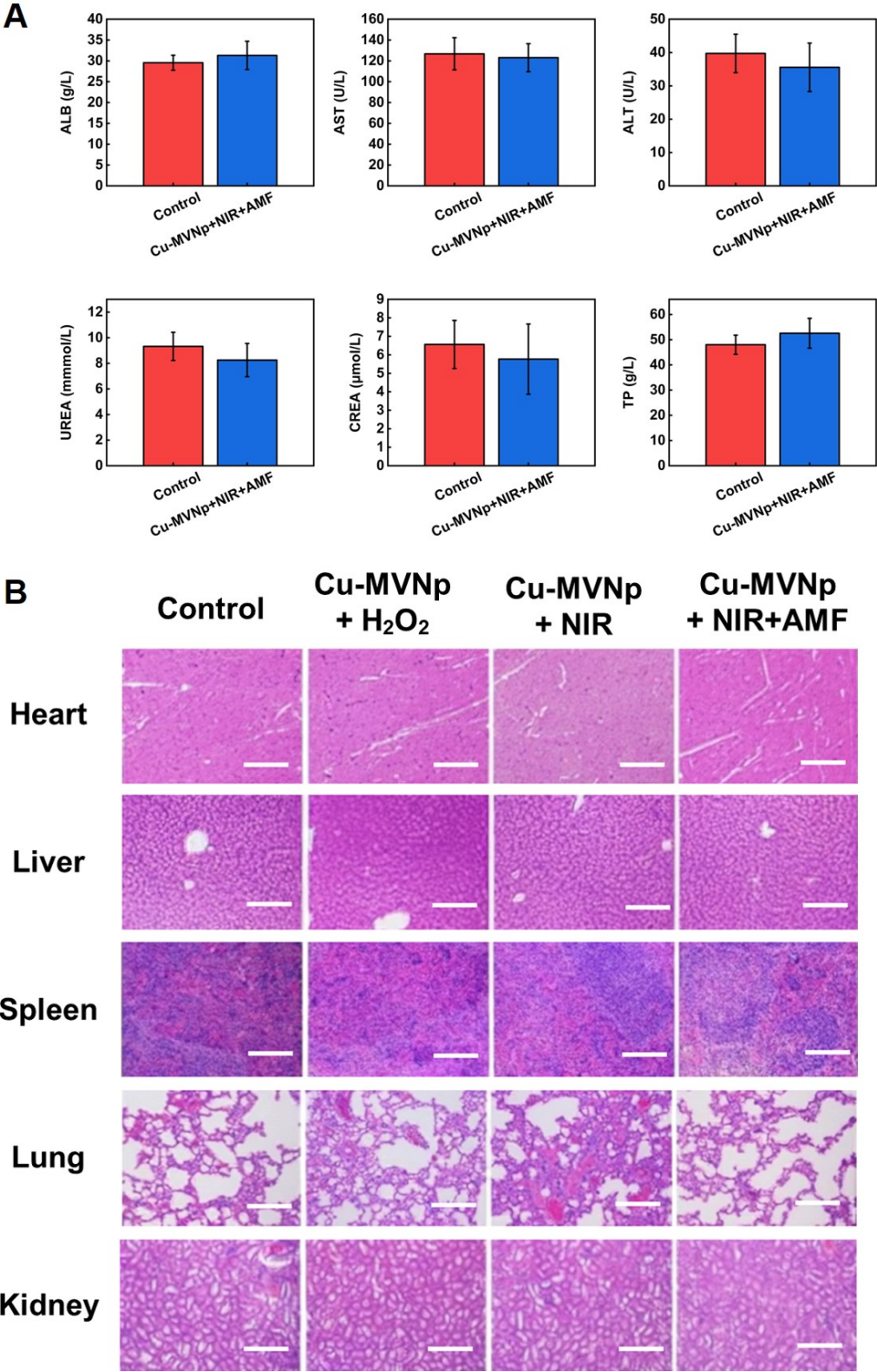
Fig. S6 (A) Biochemical markers of mice from each group on day 7 (n = 3); (B) H&E staining of major organs (heart, liver, spleen, lung, kidney) from mice in each group on day 7 (Scale bars: 200 μm).

S8: Transcriptomic analysis of the effect of tri-therapy on bacterial gene expression
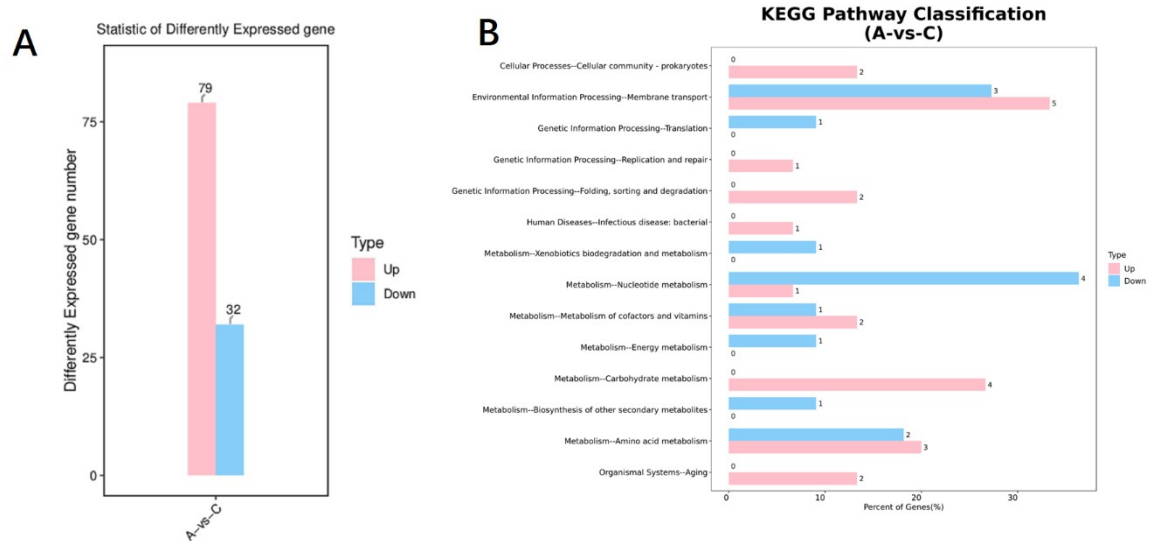
Fig. S7 (A) Distribution map showing upregulated and downregulated differentially expressed genes at KEGG Level 2 (A represents the Cu-MVNp+H_2O_2+NIR+AMF treatment group; C represents the Control group); (B) KEGG pathway classification: The horizontal axis shows the percentage (%) of upregulated or downregulated differentially expressed genes annotated to each Level 2 pathway relative to the total number of such genes. The vertical axis lists the names of the Level 2 pathways. The numbers adjacent to the bars indicate the count of upregulated or downregulated differentially expressed genes associated with each Level 2 pathway.

S9: The stability of Cu-MVNp in physiological environments
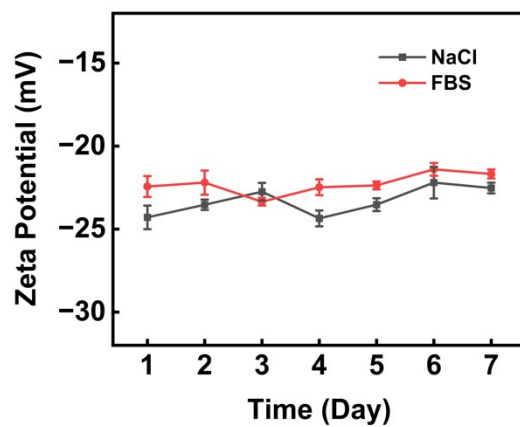
Fig. S8 Zeta potential of Cu-MVNp in NaCl and FBS (Fetal Bovine Serum).

Reference

1   W. Ren, Y. Yan, L. Zeng, Z. Shi, A. Gong, P. Schaaf, D. Wang, J. Zhao, B. Zou, H. Yu, G. Chen, E. M. B. Brown and A. Wu, *Advanced Healthcare Materials*, 2015, **4**, 1526-1536.